Characterization of Electroless Ni–P Coating Prepared on a Wrought ZE10 Magnesium Alloy

Martin Buchtík [1],* [ID], Petr Kosár [1], Jaromír Wasserbauer [1], Jakub Tkacz [1] [ID] and Pavel Doležal [1,2] [ID]

1   Materials Research Centre, Faculty of Chemistry, Brno University of Technology, Purkyňova 464/118, 612 00 Brno, Czech Republic; xckosarp@fch.vut.cz (P.K.); wasserbauer@fch.vut.cz (J.W.); tkacz@fch.vut.cz (J.T.); dolezal@fme.vutbr.cz (P.D.)
2   Faculty of Mechanical Engineering, Brno University of Technology, Technická 2896/2, 602 00 Brno, Czech Republic
*   Correspondence: xcbuchtik@fch.vut.cz; Tel.: +420-736-445-019

Abstract: Electroless low-phosphorus Ni–P coating was deposited on a wrought ZE10 magnesium alloy including an advanced pre-treatment of the material surface before deposition. Uniform Ni–P coating with an average thickness of 10 μm was formed by 95.6 wt % Ni and 4.4 wt % P. The content of Ni and P was homogeneous in the entire cross-section of the coating. Applying the Ni–P coating to the magnesium substrate, the surface microhardness increased from 60 ± 4 HV 0.025 to 690 ± 30 HV 0.025. Using the scratch test, it was determined that deposited Ni–P coating exhibits a high degree of adhesion to the magnesium substrate. Electrochemical corrosion properties of Ni–P coating were analyzed using the polarization tests in 0.1 M NaCl, while the deposited Ni–P coating showed an improvement of the corrosion resistance when compared to the ZE10 magnesium alloy. Using the scanning electron microscopy analysis, it was determined that the fine morphology of the deposited Ni–P coating did not contain visible microcavities. The absence of macrodefects due to the adequate pre-treatment before coating was reflected on the mechanism of the coated ZE10 degradation in a 0.1 M NaCl solution.

1. Introduction

Magnesium alloys are ranked among the lightest constructional metallic materials [1,2]. They find their application in the automotive and aerospace industry due to their low density and high value of specific strength, toughness, and good machinability [3]. Low corrosion resistance, high chemical reactivity, low hardness, and low wear and abrasion resistance are considerable disadvantages of magnesium-based materials [4].

Mg–Zn–RE-based magnesium alloys such as ZE10 and ZE41 achieve higher values of strength and better mechanical and corrosion properties in comparison with pure magnesium [2,5]. These alloys contain, besides Mg, Zn, and rare earth (RE) elements, Pr, Nd, La, Ce, and a small amount of Zr [1]. Zinc improves the strength and corrosion resistance of magnesium alloys. Rare earth elements improve the casting and mechanical properties (strength and creep resistance) of the alloys at higher temperatures. Zr is mainly used for grain refinement [1,6]. Although these alloys achieve better mechanical and corrosion properties in comparison with pure magnesium, their surface properties such as hardness, corrosion, and wear resistance are still inadequate for certain industrial applications.

There are several ways to improve magnesium alloys surface properties and resistivity, including galvanic or electroless deposited coatings, thermally sprayed coatings, and applications of conversion coatings [7,8].

One way to protect the material from corrosion, and improve the material surface's mechanical properties, is to apply electroless Ni–P coatings in a nickel bath [9]. Electroless deposited Ni–P coatings increase corrosion resistance as well as the surface's mechanical properties such as hardness and wear resistance. Applied low-phosphorus Ni–P coatings, compared with high-phosphorus Ni–P coatings, have a high value of hardness, a high density, and a high crystallinity [10]. However, the deposited high-phosphorus Ni–P coatings have higher corrosion resistance when compared to the low-phosphorus Ni–P coatings. Based on the phosphorus content in Ni–P coatings, low-, medium-, and high-phosphorus Ni–P coatings can be distinguished. Low-phosphorus Ni–P coatings contain 2–5 wt % phosphorus, medium-phosphorus Ni–P coatings contain 6–9 wt % phosphorus, and high-phosphorus Ni–P coatings contain >10 wt % phosphorus [9,11].

In [12], the corrosion behavior of three types of electroless deposited Ni–P coatings was studied. Ni–P coatings deposited on the mild steel contained 3.34% P (low phosphorus), 6.70% P (medium-phosphorus), and 13.30% P (high phosphorus). Based on the obtained results of potentiodynamic polarization tests and Nyquist plots of deposited Ni–P coatings in a 3.5% NaCl solution, it was determined that corrosion potentials and charge transfer resistances (in this case, equal to the polarization resistance) of deposited Ni–P coatings increased as phosphorus content increased. Corrosion potential E_{corr} of the low-phosphorus Ni–P coating obtained using the Tafel extrapolation method was −536 mV, and charge transfer resistance R_{ct} was 6.90 kΩ·cm². Corrosion potentials for medium- and high-phosphorus Ni–P coatings were −434 mV and −411 mV, respectively. Charge transfer resistances of medium- and high-phosphorus coatings were 24.86 kΩ·cm² and 37.45 kΩ·cm², respectively.

The adhesion of the coating to the substrate has a great influence on corrosion behavior and the mechanical properties of Ni–P coatings deposited on the substrate [10]. The adhesion of the Ni–P coating to the deposited substrate is significantly affected by appropriately selected pre-treatment of the substrate surface, such as grinding, blasting, degreasing, pickling, and interlayer deposition. [7,9,13]. A very frequent type of pre-treatment is zincate-zinc immersion [14–16], but the main disadvantage is the high pH value [14–17]. Zinc immersion is used to remove residual oxides and hydroxides from the surface of the substrate [14].

This paper deals with the preparation and characterization of an electroless deposited Ni–P coating deposited on a wrought ZE10 magnesium alloy. This study is focused on the measurement and evaluation of mechanical, physical, and corrosion properties of the coated substrate, while a specific pre-treatment was used before substrate coating. The mechanism of the corrosion attack and the corrosion resistance of the coated and plain material in 0.1 M NaCl were studied using potentiodynamic tests and immersion tests, and the results were analyzed in terms of light microscopy and scanning electron microscopy.

2. Materials and Methods

Wrought ZE10 magnesium alloy samples with dimensions of 20 × 20 × 1.6 mm³ were used as a substrate material for deposition of the electroless Ni–P coating. The microstructure of the ZE10 magnesium alloy, shown in Figure 1, was characterized using the light microscopy (LM) and the individual microstructural features were identified using a Zeiss EVO LS-10 scanning electron microscope (SEM, Carl Zeiss Ltd., Cambridge, UK) with an energy-dispersive X-ray spectroscopy (EDS) Oxford Instruments Xmax 80 mm² detector (Oxford Instruments plc, Abingdon, UK) and AZtec software analysis (version 2.4). Elemental composition of the coated material shown in Table 1 obtained using the GDOES (glow-discharge optical emission spectroscopy) corresponds to the ASTM standard [18].

To reveal the ZE10 magnesium alloy microstructure, prepared and polished metallographic samples were poured into an acetic picral etchant (consisting of 4.2 g of picric acid, 10 mL of acetic acid, 10 mL of distilled water, and 70 mL of ethanol) for 3 s and then into 2% Nital for 1 s [19]. The microstructure of the substrate, characterized on the surface parallel to the material processing,

was formed by solid solution grains of α-Mg, Mg_7Zn_3(RE) (La, Ce)-based particles and undissolved Zr particles (Figure 1b) [1,5]. Via EDS analysis, the presence of Ce, La, Pr, and Nd elements was found in the Mg_7Zn_3(RE) (La, Ce)-based particles.

Table 1. The elemental composition of the wrought ZE10 magnesium alloy (wt %) (GDOES).

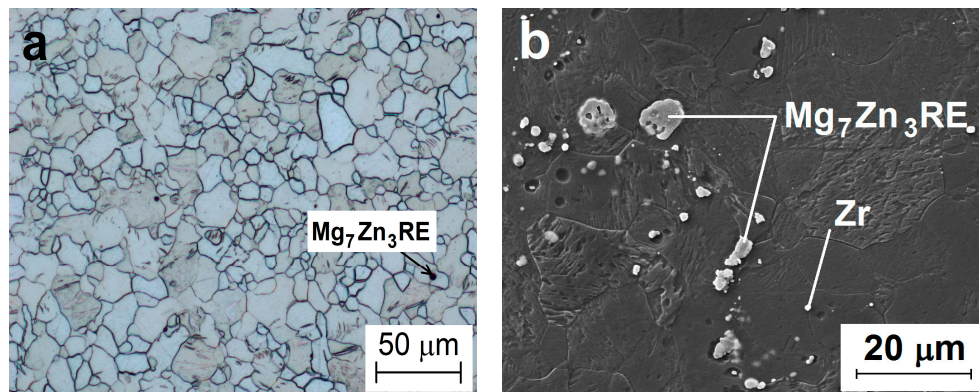| Zn	Zr	Mn	Fe	Mg	Others
1.41	0.14	0.08	0.005	balance	max. 0.30

Figure 1. Surface microstructure of the ZE10 wrought magnesium alloy: (**a**) microstructure (LM); (**b**) intermetallic phase particles in microstructure (SEM).

To achieve a sufficient activity and roughness of the magnesium substrate surface before electroless Ni–P coating deposition, a suitably chosen specific pre-treatment is required. First, the samples were ground using SiC paper no. 1200 and then cleaned in an alkaline degreasing bath with the content of soil-releasing agents. To activate the magnesium substrate surface by partial etching, pickling in an acid pickling bath based in acetic acid was performed. Partial etching of the substrate surface led to an increase in the surface roughness and activity. This process was shown to have a positive influence on adhesion and mechanical properties of deposited Ni–P coating due to the mechanical interlocking of deposited Ni–P coating to magnesium substrate [20].

The electroless nickel bath contained a nickel source, $NiSO_4 \cdot 6H_2O$, a reducing agent, $NaH_2PO_2 \cdot H_2O$, a complexing agent, and the substance-activating NaH_2PO_2 molecule. Samples were localized in the middle of the nickel bath to ensure uniform coating creation and the elimination of the thermal gradient from the bath surface [9]. The deposition of the electroless Ni–P coating proceeded for 60 min. For the microhardness measurement, a thicker coating was required, so a time of 180 min was taken for the coating preparation.

The distribution and the average content of nickel and phosphorus in deposited Ni–P coatings were determined using the Zeiss EVO LS-10 with an EDS Oxford Instruments Xmax 80 mm^2 detector SEM and the AZtec software (version 2.4). SEM observations were used to characterize Ni–P coating surface morphology and for the evaluation of the mechanism of corrosion degradation of the magnesium substrate with the subsequent violation of Ni–P coating after exposition in 0.1 M NaCl.

The microhardness measurement of the deposited Ni–P coating was carried out using the LECO AMH43 microhardness tester (Saint Joseph, MO, USA). The average value of the microhardness was obtained from 10 valid indentations performed within the coating cross section under the applied load of 25 g for 10 s, according to the ASTM E384 standard [21]. The indents were performed parallel to the coating surface.

Physical properties of the electroless deposited Ni–P coating were evaluated using the REVETEST scratch tester CSM Instruments with the Rockwell diamond indenter with a top angle of 120 and 200 µm radius hemispherical tip [22]. The progressive load type method was applied to the measurement.

The substrate surface was polished to the roughness of $R_a \approx 2$ μm using a DP-Paste M (diamond paste from Struers, Ballerup, Denmark) during the pre-treatment process before the alkaline degreasing in the addition. The friction force, the friction coefficient, the penetration depth, and the acoustic emission were recorded during the scratch test. Normal force was recorded. The applied normal force was set up in the range from 1 to 20 N. The speed of indenter was 1.58 mm·min^{-1}, and the total length of the trace was 3 mm.

The electrochemical corrosion characteristics of the ZE10 magnesium alloy and material with deposited Ni–P coating were analyzed in a 0.1 M solution of NaCl using the Bio-Logic VSP-300 potentiostat/galvanostat (BioLogic, Seyssinet-Pariset, France). Electrochemical polarization tests were performed on three specimens. A standard three-electrode cell was used for the measurements: a Pt gauze was used as a counter-electrode, a saturated calomel electrode (SCE) as a reference electrode, and a prepared sample as a working electrode. The analyzed sample area exposed to the solution during the polarization test was 1 cm^2. The stabilization time of the samples exposed to the corrosive environment was 5 min. The polarization range of the measurements was from -50 to $+200$ mV vs. open circuit potential (OCP). The corrosion potential E_{corr} and the corrosion current density i_{corr}, were determined applying the Tafel analysis, and the corrosion rate v_{corr} was calculated from the i_{corr}, according to the literature [23].

For the evaluation of the mechanism of the corrosion degradation of the ZE10 magnesium substrate with subsequent violation of the deposited Ni–P coating, the sample was immersed in the 0.1 M NaCl for 1 h. After this time, the rinsed and dried surface of the samples was analyzed via SEM.

3. Results and Discussion

3.1. Ni–P Coating Morphology and Chemical Analysis

Uniform Ni–P coating was successfully deposited on the previously pre-treated surface of the ZE10 magnesium alloy substrate. As shown in Figure 2a, grain boundaries and intermetallic phase particles appeared on the surface of the material after the pre-treated, pickled substrate. The pickled surface also shows a "honeycomb-like microstructure." Revealed intermetallic phase particles/α-Mg solid solution interface and the grain boundaries served as places where the initiation of the electroless deposition of the coating initiated due to the galvanic coupling [24]. The higher roughness of pickled and activated surface increased the adhesion of deposited Ni–P coating to the magnesium substrate.

Usually, zinc immersion is used for the magnesium alloy pre-treatment before Ni–P coating deposition. El Mahallawy et al. [14] studied the electroless Ni–P coating of different magnesium alloys, using zinc immersion as the pre-treatment of magnesium alloys. The zinc immersion was used to remove the residual oxides and hydroxides from the surface of the magnesium alloys, and a thin layer of zinc formed on the Mg surface preventing back oxidation.

Based on the obtained results, a partial re-oxidation of the ZE10 magnesium alloy surface occurred without the use of zinc immersion (Figure 2a). During the following immersion of the activated sample into the electroless nickel bath, the substrate became catalytically active when the surface oxides were dissolved in the nickel bath, and the replacement reaction occurred between the substrate and nickel ions. Even though some contamination of the substrate surface was observed before Ni–P coating deposition, it seems that it did not negatively affect the coating process [9].

The surface morphology of the deposited Ni–P coating with a nodular structure, formed by typical cauliflower-like shapes is shown in Figure 2b. Wang et al. [25] showed that deposited Ni–P coatings are formed by a columnar microstructure. However, the deposited Ni–P amorphous coatings improve the corrosion resistance of magnesium, the inherent columnar microstructure of the coating does not provide the best protection against the corrosion. The high concentration of inter-column defects, such as microvoids and micropores, [26,27], form channels where the corrosion ions and environment can pass through the coating and react with the substrate. The presence of microcavities was not evident between nodular cusps of the deposited coating (Figure 2b), which is in agreement

with observations in [28]. Based on an evaluation of SEM figures (Figures 2b and 3a), no defects and cracks were observed in the deposited Ni–P coating at the ZE10 magnesium substrate/Ni–P coating interface.

The average thickness of the coating prepared for 60 min determined from the cross sections was approximately 10 μm. In the case of a longer deposition time (180 min), prepared with the aim to increase the coating thickness to obtain relevant microhardness values, thickness was 30 μm.
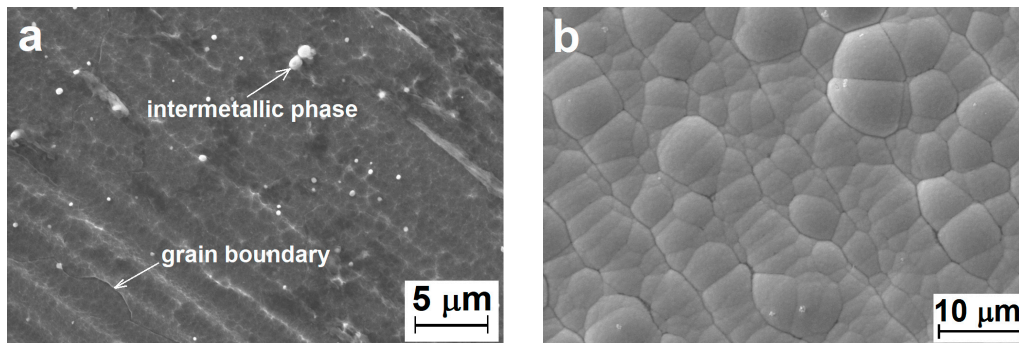

Figure 2. SEM microstructure of the pre-treated substrate and deposited Ni–P coating: (**a**) pre-treated surface of the ZE10 magnesium alloy before deposition; (**b**) fine morphology of the deposited Ni–P coating.

Deposited Ni–P coating with an average thickness of about 10 μm was chosen for EDS analysis (Figure 3). Using EDS mapping analysis, it was determined that the distribution of Ni and P in deposited Ni–P coating was homogeneous in the entire cross section, as shown in Figure 3b,c, respectively. The EDS analysis determined that the Ni content in the deposited Ni–P coating was 95.6 wt % and the P content was 4.4 wt %. Based on the literature [9,29], it was determined that the deposited Ni–P coating is low-phosphorus, as in the cases of the AZ31 magnesium alloy presented in [30] and the AZ61 magnesium alloy in [28].
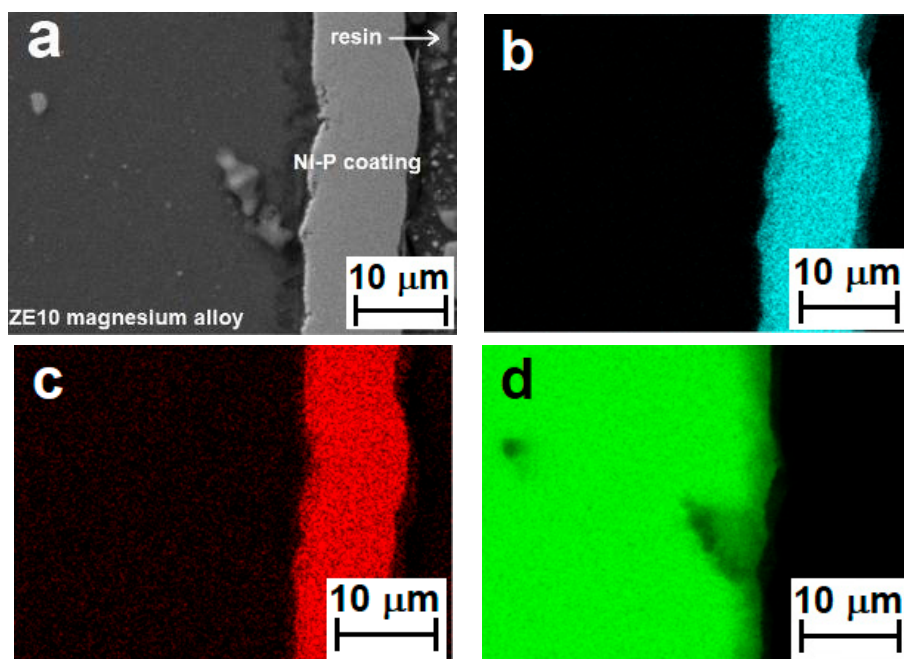

Figure 3. EDS analysis of deposited Ni–P coating on the ZE10 magnesium alloy: (**a**) a cross section of the Ni–P-coated sample, (**b**) nickel, (**c**) phosphorus, and (**d**) magnesium.

3.2. Ni–P Coating Microhardness Analysis

Based on the measured data, it was determined that the average value of the microhardness of the Ni–P coating was 690 ± 30 HV 0.025, measured in the cross section. The microhardness of the plain ZE10 magnesium substrate was 60 ± 4 HV 0.025.

The surface microhardness of the coated samples increased approximately 11-fold compared with the ZE10 magnesium alloy.

It is assumed that the measured hardness of low-phosphorus Ni–P coatings is higher compared to the high-phosphorus coatings [9]. The addition of filler (SiC, Al_2O_3) into the high-phosphorus Ni–P matrix led to a substantial increase in hardness [9]. The microhardness (690 ± 30 HV 0.025) of the deposited low-phosphorus Ni–P coating on the ZE10 magnesium alloy reached a value higher than that of the Ni–P/SiC composite coating prepared on the AZ91 magnesium alloy presented in [31] and [32]. The microhardness of the Ni–P/SiC composite coating (7.33 wt % P) was 620 HV [31], and that of the electroless Ni–P/SiC nanocomposite coating (10 wt % P) was 600 HV 0.025 [32].

The microhardness of the deposited low-phosphorus Ni–P coating was higher compared with the values obtained for the high-phosphorus Ni–P coatings. The hardness of high-phosphorus Ni–P coatings ranges from 410 to 600 HV [29,33]. As the content of phosphorus in Ni–P coatings increases, the microhardness of the coating decreased due to the microstructural changes (a decrease in crystallinity) [9].

3.3. Analysis of the Physical Properties of the Ni–P Coating

The results of the scratch test performed on the Ni–P-coated ZE10 magnesium alloy sample are shown in Figure 4. The measured values of the critical normal forces L_{c1} and L_{c2} and the corresponding friction forces F_{t1} and F_{t2}, respectively, are given in Table 2. As indicated by Table 2, the value of the critical normal force L_{c1} was 7.9 N, and the formation of oblique and parallel cracks was observed on the coating surface (Figure 5a). The value of the critical normal force L_{c2} was 13.6 N, and the formation of transverse tensile arch cracks across the entire width of the track was observed on the coating surface (Figure 5b).
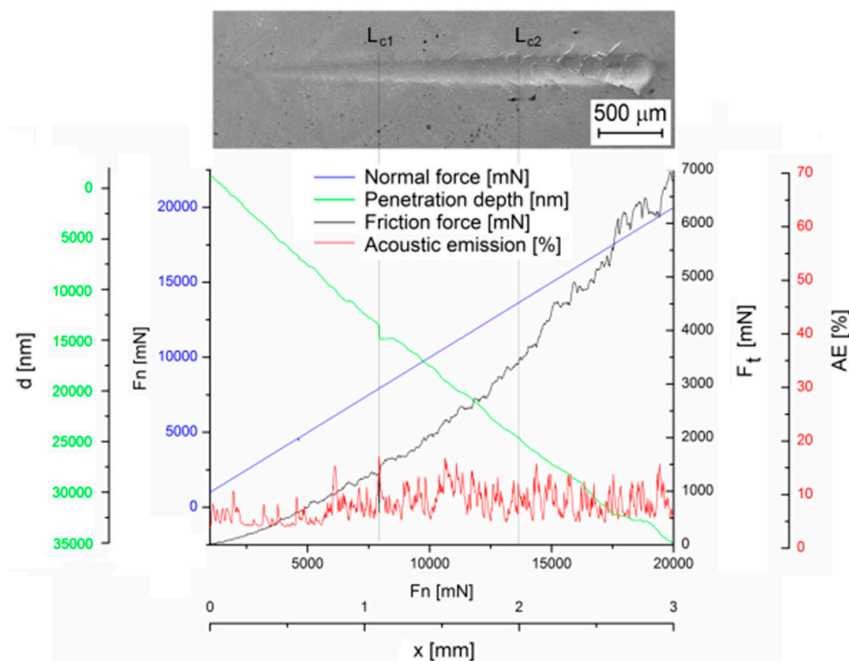

Figure 4. Results of the scratch test for the Ni–P coating on the ZE10 magnesium alloy with a scratch pattern.

As stated in [22], tensile and compressive stresses are generated during the scratch test and cause more complex mechanisms and damage. A crack can nucleate on a defect or at the coating/substrate interface. The crack is formed due to the localization of the stresses on the coating/substrate interface or in the coating (transverse crack). In the case of a layer, the tensile radial tension induced with the Rockwell tip can generate circular or transverse arch cracks that extend across the layer into the substrate. As the tip moves, several circular or transverse arch cracks can intersect. These cracks can also occur at the back of the contact as a response to tensile stresses during tip sliding. Cracks also occur on the back of the contact due to the friction-induced tensile stresses [34].

Table 2. Values of critical normal forces and friction forces of Ni–P coating deposited on the ZE10 magnesium alloy and, for comparison, values found in other studies.

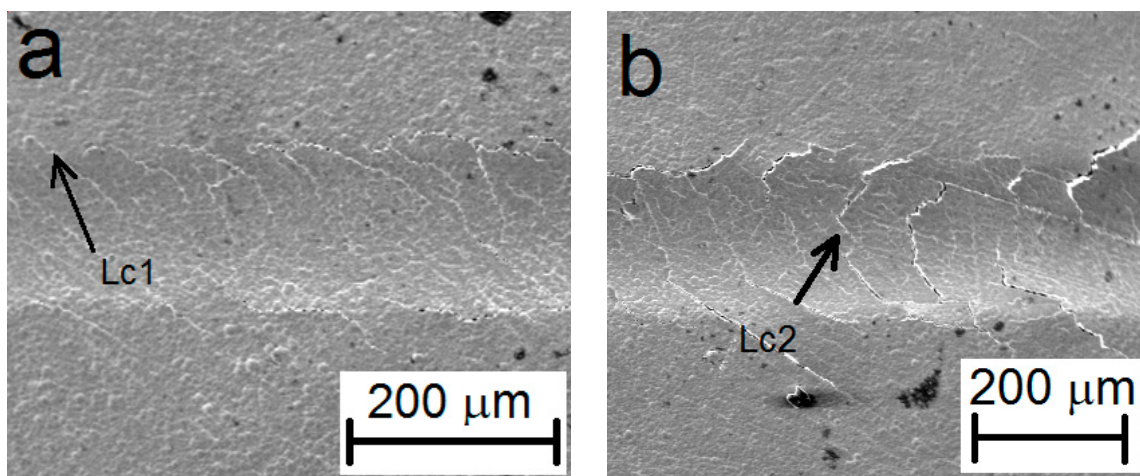| Source	Substrate	Coating	L_{c1} [N]	L_{c2} [N]	F_{t1} at L_{c1} [N]	F_{t2} at L_{c2} [N]
presented Ni–P coating	ZE10	Ni–P	7.9	13.6	0.6	3.4
[30]	AZ31	Ni–P	7.3	12.3	1.1	2.6
[28]	AZ61	Ni–P	6.9	11.9	0.8	2.2
[35]	Polished AZ91	Ni–P	–	10.2 (L_c)	–	–
		Ni–P (temp.: 523 K)	–	10.6 (L_c)	–	–
		Ni–P (temp.: 673 K)	–	9.7 (L_c)	–	–
[35]	Blasted AZ91	Ni–P	–	14.0 (L_c)	–	–
		Ni–P (temp.: 523 K)	–	16.5 (L_c)	–	–
		Ni–P (temp.: 673 K)	–	14.8 (L_c)	–	–
[36]	AISI 1018	plain Ni–P/TiO_2	–	~13 (L_c)	–	–
		Ni–P/TiO_2 with SDS	–	~19 (L_c)	–	–
		Ni–P/TiO_2 with DTAB	–	~29 (L_c)	–	–

Figure 5. Detail of the damage of Ni–P coating during the scratch test: (**a**) L_{c1} and (**b**) L_{c2} (SEM).

As a result of the applied pressure load of the Rockwell diamond tip during the scratch test, ductile failure of the deposited Ni–P coating occurs due to the introduced internal stresses.

The character of the damage to the locating layer during the scratch test is dependent on many factors [22]. In addition to the influence of the characteristics of the experimental device on the tested layer damage mechanism, there are geometric properties of the substrate-layer system (such as layer thickness, roughness, etc.), experimental parameters (tip and scratch rate), and properties of the substrate-layer system (thermal coefficients, microstructure and internal stresses, elasticity, and hardness modules). Figures 4 and 5 show the scratch track morphology and the layer cracking character, which is similar to the case of Ni–P coatings on AZ31 and AZ61 magnesium alloys presented in [28,30].

The formation of transverse tensile arch cracks [22,34] across the entire width of the track was observed (Figure 4). The adhesion strength of the experimental electroless deposited Ni–P coating on a wrought ZE10 magnesium alloy (L_{c1} and L_{c2}) was higher compared to the data presented in articles [28,30], where the Ni–P coating was deposited on AZ31 and AZ61 magnesium alloys, respectively. The difference could be explained by the coated substrate pre-treatment process. The pre-treatment of AZ31 and AZ61 magnesium alloys before the deposition of the Ni–P coating included polishing to a roughness $R_a \approx 0.25$ μm [28,30]. However, the surface of the experimental ZE10 magnesium alloy was polished to a roughness $R_a \approx 2$ μm, which is significantly rougher than AZ31 and AZ61. The higher roughness of the substrate surface can improve the adhesion strength between the deposited Ni–P coating and the ZE10 magnesium alloy due to the mechanical interlocking of the two components [34].

This effect was also observed in [35], where the adhesion strength between the deposited Ni–P coating and blasted or polished surface of the AZ91 magnesium alloy was studied. The scratch track morphology for the pre-blasted and pre-polished samples with the deposited Ni–P coating showed a similar trend, but it was observed that the scratch track width was narrower on the rougher surface when compared to the polished surface. The scratch track width was slightly narrower for coated samples after annealing for 1 h at 523 K. This effect can be contributed to the increase in the hardness of the Ni–P coating after annealing, which was demonstrated with the increase in hardness from ~600 to ~900 HV due to the coated sample annealing. As indicated by Table 2, the critical load L_c for the plain Ni–P coating was 14.0 N and 10.2 N for the blasted and polished surfaces, respectively. The increase in adhesion strength to 16.5 N was observed for the rough blasted AZ91 substrate after annealing for 1 h at 523 K. This increase was apparently linked to the hardness increase and the effect of the rough surface. The brittle cracking of the deposited coating was observed at substrates with the rough surface, and the wedge spallation was observed at substrates with the polished surface. The decrease in adhesion strength was observed for samples annealed at 673 K due to the embrittlement of the Ni–P coatings (Table 2).

However, as indicated by Table 2, resulting values of the critical loads of rough (blasted) samples of AZ91 [35] are slightly higher when compared to the experimental Ni–P coating deposited on the ZE10 magnesium alloy. This can again be connected to the higher roughness of the coated substrate. The roughness of the blasted AZ91 magnesium alloy surface was $R_a \approx 4.5$ μm [35], and that of the experimental ZE10 magnesium alloy was $R_a \approx 2$ μm. It is also possible to observe that the value of the critical load L_c of experimental coating deposited on the ZE10 alloy is higher in comparison with the polished surface of the AZ91 alloy in [35], where the roughness was $R_a \approx 0.05$ μm. As is obvious, the roughness of the substrate surface has a significant effect on the coating adhesion strength due to the mechanical interlocking between Ni–P coating and the coated magnesium substrate.

As indicated in the literature [36], applied surfactants in the nickel bath had a significant effect on the adhesion strength of deposited Ni–P/TiO$_2$ composite coating on the AISI 1018 steel substrate (Table 2). No cohesive or adhesive failure of the coating was observed up to ~13 N in the case of the Ni–P/TiO$_2$ coating prepared on AISI 1018 without using the surfactant. The formation of the mild tensile cracks at ~19 N was evident for the Ni–P/TiO$_2$ composite coating using sodium dodecyl sulfate (SDS) surfactant at 1.5× CMC (critical micelle concentration). In the case of the Ni–P/TiO$_2$ composite coatings on AISI 1018 involving dodecyl trimethyl ammonium bromide (DTAB) at 1× CMC, the cohesive failure was observed at the applied load of ~29 N. Moreover, no linear or radial cracks were observed in the case of the coated steel substrate, nor of any of the analyzed coatings, which also indicates the importance of the surface of the substrate with respect to the adhesion of the coating.

The increase in the adhesion strength of Ni–P coatings to the magnesium substrate, along with a slight increase in the roughness of the substrate surface, was shown to be achieved by adding the proper surfactant into the nickel bath [35,37]. This proves that a more effective adhesion of the coatings is caused by the excessive attractive forces between the Ni–P coatings and substrate [38].

Based on the obtained result, a sufficient surface roughness of ZE10 reached via surface polishing on the roughness $R_a \approx 2$ µm, in combination with the activation of the surface via acid pickling, seems to be reached during pre-treatment. Adequate pretreatment resulted in an adequate adhesion of the coating to the substrate and a considerably high resistivity against damage.

3.4. The Electrochemical Corrosion Test in 0.1 M NaCl

Figure 6 shows the potentiodynamic polarization curves of the ZE10 magnesium alloy and the ZE10 alloy with the deposited Ni–P coating in 0.1 M NaCl obtained at laboratory temperature. The polarization curve of the Ni–P-coated sample is significantly shifted to more electropositive values, which means better corrosion properties of the Ni–P-coated sample compared with the untreated ZE10 magnesium alloy.

Therefore, a deposited Ni–P coating appears to be suitable for the protection of magnesium alloys. Based on the Tafel extrapolation analysis [39], the values of the corrosion potential, E_{corr}, and the corrosion current density, i_{corr}, for samples with the deposited Ni–P coating and the ZE10 magnesium alloy were determined. The average values of the E_{corr}, for the ZE10 magnesium alloy and the Ni–P-coated alloy, were −1701 and −505 mV, respectively, and the values of the i_{corr}, for the ZE10 magnesium alloy and the Ni–P-coated material, were 23.7 and 0.4 µA·cm^{-2}, respectively (Table 3). It is generally known [25] that the columnar structure of deposited Ni–P coatings contains a network of defects (grain boundaries, pores, and microcavities). These defects are precursors for a micropitting and may cause the corrosion attack of the material under the deposited Ni–P coating. However, no local corrosion attack (pitting) was observed in the anodic area of the polarization curves.

Based on the determined values of i_{corr}, the corrosion rate, v_{corr}, was calculated for a short-term experiment. As indicated by Table 3, the corrosion rates of the ZE10 alloy and the Ni–P-coated samples in 0.1 M NaCl were 530.00 µmpy and 8.95 µmpy, respectively.

Experimental deposited Ni–P coating was ranked among the low-phosphorus Ni–P coatings, which are characterized by their lower corrosion resistance when compared to the medium- and high-phosphorus coatings, [9]. As indicated in the work of S. Narayanan [12], deposited Ni–P coatings with low phosphorus content (3.34 wt % P) showed an E_{corr} of −0.536 V and an i_{corr} of 4.22 µA·cm^{-2}, whereas medium- (6.70 wt % P) and high-phosphorus (13.30 wt % P) Ni–P coatings showed E_{corr} values of −0.434 and −0.411 V, respectively, and i_{corr} values of 1.17 and 0.60 µA·cm^{-2}, respectively. When comparing the experimentally obtained results and the results presented in [12], it is evident that the value (Table 3) of the corrosion potential, E_{corr}, is between E_{corr} values of 25-µm-thick low-phosphorus (3.34 wt % P) and medium-phosphorus (6.70 wt % P) Ni–P coatings presented in [12].

Table 3. Corrosion parameters of the ZE10 magnesium alloy and the ZE10 alloy with a deposited Ni–P coating.

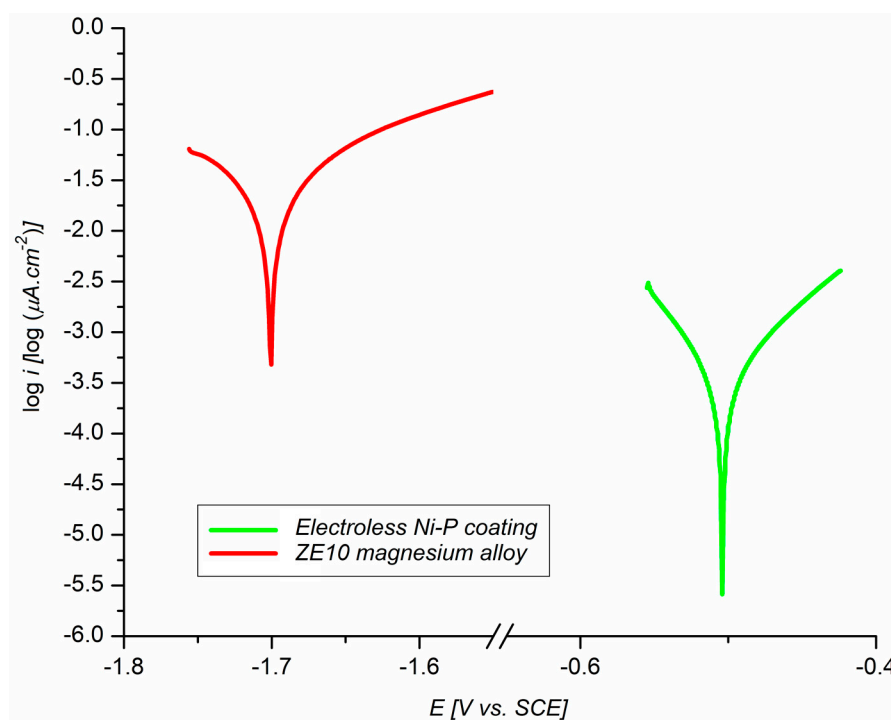| Sample	E_{corr} [mV]	i_{corr} [µA·cm^{-2}]	v_{corr} [µmpy]
ZE10 alloy	−1701	23.7	530.00
ZE10 + Ni–P coating	−505	0.4	8.95

Figure 6. Characteristic potentiodynamic polarization curves for the ZE10 magnesium alloy and the ZE10 alloy with a deposited Ni–P coating in 0.1 M NaCl obtained at laboratory temperature.

Although the plating rate of high-phosphorus Ni–P coatings in [12] was higher, high-phosphorus Ni–P coatings were deposited under more energy-intensive conditions (90 ± 1 °C) [12]. It is evident that the obtained value of the corrosion current density, i_{corr}, of high-phosphorus Ni–P coating was worse compared to the presented low-phosphorus Ni–P coatings on the ZE10 magnesium alloy (Table 3), and the electroless deposited coating on the ZE10 alloy exhibits greater corrosion resistance. This can be attributed to the fact that the experimentally prepared electroless deposited Ni–P coating was probably less defective or that the Ni–P coating contained only a small amount of microcavities when compared to the coatings analyzed in [12].

3.5. The Immersion Test in 0.1 M NaCl

As indicated by Figure 7a,b, after the exposition of the sample with deposited Ni–P coating in 0.1 M NaCl for 1 h, the degradation of the Ni–P coating occurred due to the corrosion of the magnesium substrate under the coating.

Corrosive agents may accumulate between the nodules (grains) creating the Ni–P coating and migrate to the substrate surface. According to the results in [25,40], the inherent columnar porous microstructure of the coating (Figure 7d) does not adequately protect the magnesium substrate against corrosive environments [41]. Furthermore, electroless Ni–P coatings contain a certain amount of microcavities in their volume. These microcavities form nucleation sites for micropitting when the material is exposed to a corrosive environment. Microcavities are created as a result of the hydrogen evolution during the deposition process when small bubbles of hydrogen H_2, as a byproduct of the nickel reduction, are adsorbed on the surface of the growing Ni–P coating [40]. Stirring of the nickel baths or the rotation of the deposited objects is a partial solution of this problem. However, the addition of surfactants into the nickel bath was shown to be a more effective solution, while the reduction of these microcavities resulted in an increase in the corrosion resistance of the coated substrate [42,43].

As described above, due to the high concentration of inter-column defects, such as microvoids and micropores [27], the interaction between the corrosive environment containing chloride ions and magnesium substrate under the deposited Ni–P coating resulted in the creation of oxides or chlorides

of magnesium. This reaction has an effect on the increase in corrosion product volume when compared to the bulk material and the evolution of hydrogen is an accompanying process. The increase in the volume of the material under the Ni–P coating leads to the formation of cracks and the subsequent destruction of the coating and thus to the acceleration of the corrosion of the magnesium substrate (Figure 7c).

Even though the coating internal defects were not observed in SEM analysis, even the intercolumnar areas can provide a path for the transfer of corrosive medium elements into the coating and react with the substrate. Figure 7d reveals the damaged structure of the Ni–P coating showing the columnar structure. The revealed columnar structure supports the theory that the grain boundaries and microdefects present on the grain boundaries acted as the paths for the corrosive medium transfer to the substrate.

Observed local corrosion attack did not correlate with the results obtained with potentiodynamic tests; however, the electrochemical test was limited to the range of polarization used, and a larger range for the measurement likely can reveal the pitting attack.
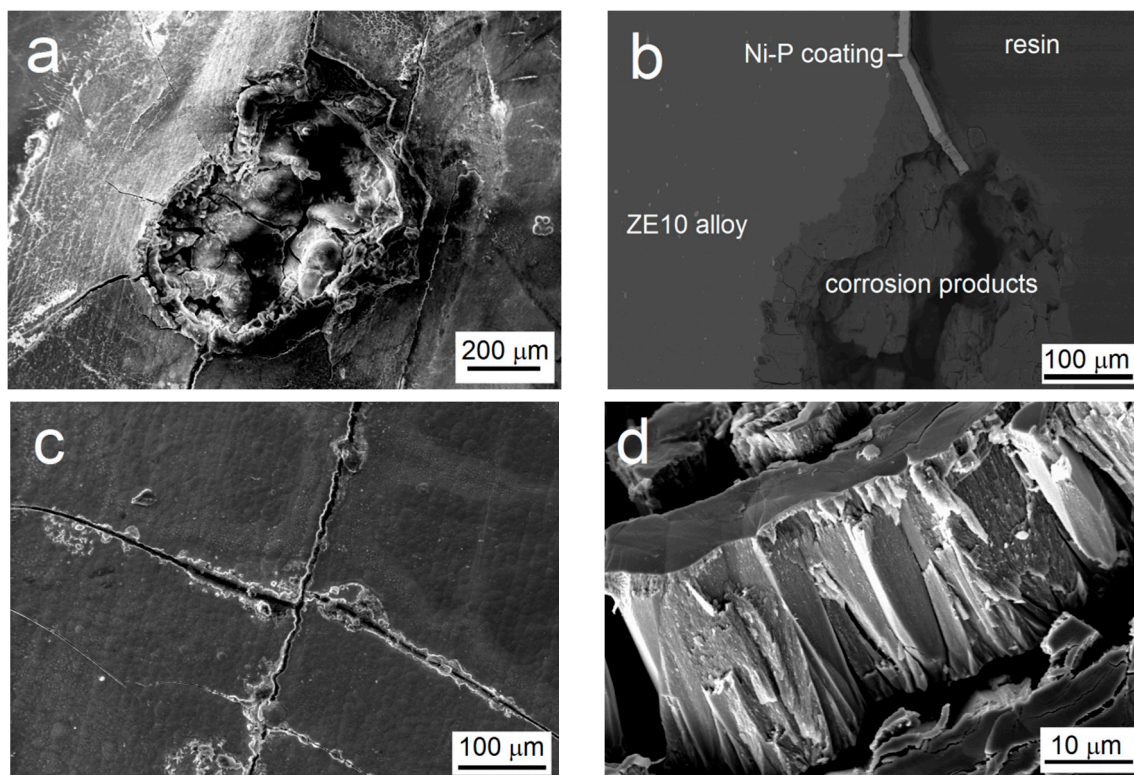

Figure 7. Corrosion degradation of the Ni–P coating on the ZE10 magnesium alloy: (**a**) surface, (**b**) cross-section, (**c**) cracks in Ni–P coating caused by the increase in volume under deposited coating due to the corrosion, (**d**) cracked Ni–P coating.

4. Conclusions

Based on the results of the characterization of the electroless deposited Ni–P coating prepared on a ZE10 magnesium alloy via polishing and acid pickling, the following conclusions can be made:

- Due to the proper pre-treatment, electroless low-phosphorus Ni–P coatings were successfully deposited on a ZE10 magnesium alloy in a nickel bath.
- The content of Ni in the deposited coatings was 95.6 wt %, and the content of P was 4.4 wt %, for coatings with average thickness ~10 μm (1 h of deposition).
- Deposited Ni–P coatings showed a high degree of homogeneity in the entire cross section.

- The microhardness of the deposited low-phosphorus Ni–P coating was 690 ± 30 HV 0.025, representing an 11-fold increase when compared to the plain ZE10 magnesium alloy.
- The adhesion of the deposited Ni–P coating was determined from the appropriate critical normal forces L_{c1} = 7.9 N, where i.e., oblique and parallel cracks are the primary failure—was observed, and L_{c2} = 13.6 N, where the formation of transverse arch cracks was observed.
- Electrochemical polarization tests have shown an improvement in corrosion resistance via the deposition of Ni–P coating (E_{corr} = −505 mV, i_{corr} = 0.4 µA·cm^{-2}, and v_{corr} = 8.95 µmpy) when compared to the ZE10 magnesium alloy (E_{corr} = −1701 mV, i_{corr} = 23.7 µA·cm^{-2}, and v_{corr} = 530 µmpy).
- Microcavities present in the coating and the columnar structure of the low-phosphorus Ni–P coating have a major influence on the process of the corrosion, acting as the channels between the corrosive environment and the substrate.

Author Contributions: Martin Buchtík designed and performed experiments; Petr Kosár prepared samples and performed experiments; Jakub Tkacz analyzed data and performed electrochemical measurement; Jaromír Wasserbauer contributed materials and analysis tools, and analyzed data; Pavel Doležal performed adhesion tests and analyzed data. Martin Buchtík wrote the paper.

Conflicts of Interest: The authors declare no conflict of interest.

References

1. Friedrich, H. Alloys Containing Zirconium. In *Magnesium Technology Metallurgy, Design Data, Automotive Applications*; Mordike, B.L., Ed.; Springer: Berlin, Germany, 2004; pp. 140–141.
2. ASM International Handbook Committee. *Properties and Selection: Nonferrous Alloys and Special-Purpose Materials*, 10th ed.; ASM International: Materials Park, OH, USA, 1990.
3. Miao, X.; Li, X.; Hu, H.; Gao, G.; Zhang, S. Effects of the Oxide Coating Thickness on the Small Flaw Sizing Using an Ultrasonic Test Technique. *Coatings* **2018**, *8*, 69. [CrossRef]
4. Shao, Z.; Cai, Z.; Hu, R.; Wei, S. The study of electroless nickel plating directly on magnesium alloy. *Surf. Coat. Technol.* **2014**, *249*, 42–47. [CrossRef]
5. Liu, Y.; Li, W.; Li, Y. Microstructure and mechanical properties of ZE10 magnesium alloy prepared by equal channel angular pressing. *Int. J. Min. Met. Mater.* **2009**, *16*, 559–563. [CrossRef]
6. Bettles, C.; Barnett, M. *Advances in Wrought Magnesium Alloys: Fundamentals of Processing, Properties and Applications*; Woodhead Publishing: Oxford, UK, 2012.
7. Fauchais, P.L.; Heberlein, J.V.R.; Boulos, M.I. *Thermal Spray Fundamentals: From Powder to Part*; Springer: New York, NY, USA, 2013.
8. Drábiková, J.; Fintová, S.; Tkacz, J.; Doležal, P.; Wasserbauer, J. Unconventional fluoride conversion coating preparation and characterization. *Anti-Corros. Method Mater.* **2017**, *64*, 613–619. [CrossRef]
9. Riedel, W. *Electroless Nickel Plating*; ASM International: Metals Park, OH, USA, 1991.
10. Mallory, G.O.; Hajdu, J.B. *Electroless Plating: Fundamentals and Applications*; Knoyes Publications/William Andrew Publishing: Norwich, NY, USA, 2009.
11. Abrantes, L.M.; Fundo, A.; Jin, G. Influence of phosphorus content on the structure of nickel electroless deposits. *J. Mater. Chem.* **2001**, *11*, 200–203. [CrossRef]
12. Sankara Narayanan, T.S.N.; Baskaran, I.; Krishnaveni, K.; Parthiban, S. Deposition of electroless Ni–P graded coatings and evaluation of their corrosion resistance. *Surf. Coat. Technol.* **2006**, *200*, 3438–3445. [CrossRef]
13. Curtis, J.M.; Polak, T.A.; Wilcox, G.D. *Handbook of Surface Treatments and Coatings*; Professional Engineering Publishing: London, UK, 2003.
14. El Mahallawy, N.; Bakkar, A.; Shoeib, M.; Palkowski, H.; Neubert, V. Electroless Ni–P coating of different magnesium alloys. *Surf. Coat. Technol.* **2008**, *202*, 5151–5157. [CrossRef]
15. Wu, L.; Zhao, J.; Xie, Y.; Yang, Z. Progress of electroplating and electroless plating on magnesium alloy. *Trans. Nonferr. Metal. Soc.* **2010**, *20*, 630–637. [CrossRef]

16. Zhou, Y.; Zhang, S.; Nie, L.; Zhu, Z.; Zhang, J.; Cao, F.; Zhang, J. Electrodeposition and corrosion resistance of Ni–P–TiN composite coating on AZ91D magnesium alloy. *Trans. Nonferr. Metal. Soc. Chin.* **2016**, *26*, 2976–2987. [CrossRef]

17. Chen, J.; Yu, G.; Hu, B.; Liu, Z.; Ye, L.; Wang, Z. A zinc transition layer in electroless nickel plating. *Surf. Coat. Technol.* **2006**, *201*, 686–690. [CrossRef]

18. *ASTM B90/B90M-15 Standard Specification for Magnesium-Alloy Sheet and Plate*; ASTM International: West Conshohocken, PA, USA, 2015.

19. Vander Voort, G.F. *Metallography, Principles and Practice*; ASM International: Materials Park, OH, USA, 1999.

20. Tran, T.N.; Yu, G.; Hu, B.N.; Xie, Z.H.; Tang, R.; Zhang, X.Y. Effects of pretreatments of magnesium alloys on direct electroless nickel plating. *Trans. IMF* **2012**, *90*, 209–214. [CrossRef]

21. *ASTM E384-17 Standard Test Method for Microindentation Hardness of Materials*; ASTM International: West Conshohocken, PA, USA, 2017.

22. *ASTM C1624-05(2015) Standard Test Method for Adhesion Strength and Mechanical Failure Modes of Ceramic Coatings by Quantitative Single Point Scratch Testing*; ASTM International: West Conshohocken, PA, USA, 2015.

23. Szewieczek, D.; Baron, A. Electrochemical corrosion and its influence on magnetic properties of $Fe_{75.5}Si_{13.5}B_9Nb_3Cu_1$ alloy. *J. Mater. Process. Technol.* **2005**, *164–165*, 940–946. [CrossRef]

24. Ambat, R.; Zhou, W. Electroless nickel-plating on AZ91D magnesium alloy: effect of substrate microstructure and plating parameters. *Surf. Coat. Technol.* **2004**, *179*, 124–134. [CrossRef]

25. Wang, W.; Zhang, W.; Wang, Y.; Mitsuzak, N.; Chen, Z. Ductile electroless Ni–P coating onto flexible printed circuit board. *Appl. Surf. Sci.* **2016**, *367*, 528–532. [CrossRef]

26. Yang, H.; Gao, Y.; Qin, W. Investigation of the Corrosion Behavior of Electroless Ni–P Coating in Flue Gas Condensate. *Coatings* **2017**, *7*, 16. [CrossRef]

27. Mao, S.; Yang, H.; Li, J.; Huang, F.; Song, Z. Corrosion properties of aluminium coatings deposited on sintered NdFeB by ion-beam-assisted deposition. *Appl. Surf. Sci.* **2011**, *257*, 5581–5585. [CrossRef]

28. Buchtík, M.; Kosár, P.; Wasserbauer, J.; Doležal, P. Characterization of Ni–P coating prepared on a wrought AZ61 magnesium alloy via electroless deposition. *Mater. Tehnol.* **2017**, *51*, 925–931. [CrossRef]

29. Parkinson, R. *Properties and Applications of Electroless Nickel*; Technical paper 10081; Nickel Development Institute: Toronto, ON, Canada, 1997.

30. Buchtík, M.; Kosár, P.; Wasserbauer, J.; Doležal, P. Characterization of Ni–P coating prepared via electroless deposition on AZ31 magnesium alloy. *Koroze a ochrana materiálu* **2017**, *61*, 1–6. [CrossRef]

31. Wang, H.-L.; Liu, L.-Y.; Dou, Y.; Zhang, W.-Z.; Jiang, W.-F. Preparation and corrosion resistance of electroless Ni–P/SiC functionally gradient coatings on AZ91D magnesium alloy. *Appl. Surf. Sci.* **2013**, *286*, 319–327. [CrossRef]

32. Farzaneh, A.; Mohammadi, M.; Ehteshamzadeh, M.; Mohammadi, F. Electrochemical and structural properties of electroless Ni–P-SiC nanocomposite coatings. *Appl. Surf. Sci.* **2013**, *276*, 697–704. [CrossRef]

33. Balaraju, J.N.; Sankara Narayanan, T.S.N.; Seshadri, S.K. Electroless Ni–P composite coatings. *J. Appl. Electrochem.* **2003**, *33*, 807–816. [CrossRef]

34. Holmberg, K.; Matthews, A. *Coatings Tribology Properties, Mechanisms, Techniques and Applications in Surface Engineering*, 2nd ed.; Elsevier Science: Amsterdam, The Netherlands, 2009.

35. Liu, Z.; Gao, W. Electroless nickel plating on AZ91 Mg alloy substrate. *Surf. Coat. Technol.* **2006**, *200*, 5087–5093. [CrossRef]

36. Tamilarasan, T.R.; Rajendran, R.; Siva shankar, M.; Sanjith, U.; Rajagopal, G.; Sudagar, J. Wear and scratch behaviour of electroless Ni–P-nano-TiO_2: Effect of surfactants. *Wear* **2016**, *346–347*, 148–157. [CrossRef]

37. Elansezhian, R.; Ramamoorthy, B.; Kesavan Nair, P. Effect of surfactants on the mechanical properties of electroless (Ni–P) coating. *Surf. Coat. Technol.* **2008**, *203*, 709–712. [CrossRef]

38. Tracton, A.A. *Coatings Technology: Fundamentals, Testing, and Processing Techniques*; CRC Press: Boca Raton, FL, USA, 2007.

39. Tkacz, J.; Minda, J.; Fintová, S.; Wasserbauer, J. Comparison of Electrochemical Methods for the Evaluation of Cast AZ91 Magnesium Alloy. *Materials* **2016**, *9*, 925. [CrossRef] [PubMed]

40. Chen, B.-H.; Hong, L.; Ma, Y.; Ko, T.-M. Effects of Surfactants in an Electroless Nickel-Plating Bath on the Properties of Ni−P Alloy Deposits. *Ind. Eng. Chem. Res.* **2002**, *41*, 2668–2678. [CrossRef]

41. Valova, E.; Georgieva, J.; Armyanov, S.; Avramova, I.; Dille, J.; Kubova, O.; Delplancke-Ogletree, M.-P. Corrosion behavior of hybrid coatings: Electroless Ni–Cu–P and sputtered TiN. *Surf. Coat. Technol.* **2010**, *204*, 2775–2781. [CrossRef]
42. Muraliraja, R.; Elansezhian, R.; Sudagar, J.; Raviprakash, A.V. Influence of a Zwitterionic Surfactant on the Surface Properties of Electroless Ni–P Coating on Mild Steel. *J. Surfactants Deterg.* **2016**, *19*, 1081–1088. [CrossRef]
43. Latt, K.M. Effects of Surfactants on Characteristics and Applications of Electroless Nickel-Phosphorous Deposits. Master's Thesis, National University of Singapore, Singapore, 2003.